FAST MAGNETOACOUSTIC WAVE TRAINS OF SAUSAGE SYMMETRY IN CYLINDRICAL WAVEGUIDES OF THE SOLAR CORONA

S. Shestov[1], V. M. Nakariakov[2], and S. Kuzin[1]
[1] Lebedev Physical Institute, Leninskii prospekt, 53, Moscow 119991, Russia; sshestov@gmail.com
[2] Centre for Fusion, Space and Astrophysics, Department of Physics, University of Warwick, Coventry CV4 7AL, UK

ABSTRACT

Fast magnetoacoustic waves guided along the magnetic field by plasma non-uniformities, in particular coronal loops, fibrils, and plumes, are known to be highly dispersive, which lead to the formation of quasi-periodic wave trains excited by a broadband impulsive driver, e.g., a solar flare. We investigated the effects of cylindrical geometry on the fast sausage wave train formation. We performed magnetohydrodynamic numerical simulations of fast magnetoacoustic perturbations of a sausage symmetry, propagating from a localized impulsive source along a field-aligned plasma cylinder with a smooth radial profile of the fast speed. The wave trains are found to have pronounced period modulation, with the longer instant period seen in the beginning of the wave train. The wave trains also have a pronounced amplitude modulation. Wavelet spectra of the wave trains have characteristic tadpole features, with the broadband large-amplitude heads preceding low-amplitude quasi-monochromatic tails. The mean period of the wave train is about the transverse fast magnetoacoustic transit time across the cylinder. The mean parallel wavelength is about the diameter of the wave-guiding plasma cylinder. Instant periods are longer than the sausage wave cutoff period. The wave train characteristics depend on the fast magnetoacoustic speed in both the internal and external media, the smoothness of the transverse profile of the equilibrium quantities, and also the spatial size of the initial perturbation. If the initial perturbation is localized at the axis of the cylinder, the wave trains contain higher radial harmonics that have shorter periods.

Key words: magnetohydrodynamics (MHD) – Sun: corona – Sun: oscillations – waves

Supporting material: animation

1. INTRODUCTION

Magnetohydrodynamic (MHD) waves with periods from several seconds to several minutes are ubiquitous in the corona of the Sun, and are intensively studied in the contexts of heating and seismology of the coronal plasma (see, e.g., De Moortel & Nakariakov 2012; Liu & Ofman 2014 for comprehensive recent reviews). Properties of MHD waves are strongly affected by field-aligned structuring of the plasma, intrinsic to the corona (e.g., Van Doorsselaere et al. 2008). Filamentation of the coronal density along the field leads to the appearance of waveguides for magnetoacoustic waves (e.g., Zajtsev & Stepanov 1975; Edwin & Roberts 1983; Roberts et al. 1984). In the waveguides fast magnetoacoustic waves become dispersive, i.e., their phase and group speeds become dependent on the frequency and wavelength. If the waves are excited by a broadband, spatially localized driver, e.g., a flare or another impulsive release of energy, induced fast magnetoacoustic perturbations develop into a quasi-periodic wave train with pronounced amplitude and frequency modulation (Roberts et al. 1984; Nakariakov et al. 2004).

The possible manifestation of fast magnetoacoustic wave trains in solar observations was first pointed out in quasi-periodic pulsations in solar radio bursts detected at 303 and 343 MHz (Roberts et al. 1983, 1984). Later on, analysis of high-cadence imaging observations of the green-line coronal emission recorded during a solar eclipse revealed the presence of similar wave trains (Williams et al. 2002; Katsiyannis et al. 2003) with the mean period of about 6 s. More recently, quasi-periodic wave trains with the periods of several tens of minutes were detected in the decametric solar emission (see Mészárosová et al. 2009, 2013; Karlický et al. 2011). Recently

discovered quasi-periodic rapidly propagating wave trains of EUV intensity, with periods from about one to a few minutes (Liu et al. 2011), are possibly associated with this phenomenon, too (Yuan et al. 2013; Nisticò et al. 2014).

Identification of the physical mechanism for the formation and evolution of coronal quasi-periodic wave trains requires advanced theoretical modeling. The initial stage of the evolution of a broadband fast magnetoacoustic perturbation in a quasi-periodic wave train was numerically simulated by Murawski & Roberts (1993, 1994). The mean period of the wave train was found to be of the order of the fast wave travel time across the waveguide, which was consistent with qualitative estimations by Roberts et al. (1983).

Nakariakov et al. (2004) modeled the developed stage of the broadband fast wave evolution in a plasma slab and found that the resultant wave train has a characteristic signature in the Morlet wavelet spectrum, the "crazy tadpole" with an narrowband extended tail followed by a broadband "head." Similar wavelet spectral signatures have been detected in observations (Mészárosová et al. 2009; Karlický et al. 2011; Yuan et al. 2013). These characteristic wavelet spectra appear in fast wave trains guided by plasma slabs with the transverse profiles of the fast speed of different steepnesses. However, it was demonstrated that the specific width of the wavelet spectral peak and its time modulation are determined by the spectrum of the initial perturbation and the cutoff wavenumber (Nakariakov et al. 2005). In particular, in some cases the effect of dispersive evolution can lead to the formation of quasi-monochromatic fast wave trains, without noticeable variation of the period. A similar behavior was established for fast wave trains guided by plane current sheets (Jelínek & Karlický 2012; Mészárosová et al. 2014). Obvious similarities of theoretical and

observational properties of coronal fast wave trains provide us with a tool for diagnostics of the wave-guiding plasma non-uniformities.

In addition, it was recently proposed that another common feature of broadband solar radio emission, fiber bursts, could also be associated with guided fast wave trains (Karlický et al. 2013). Furthermore, it was demonstrated that modulations of broadband radio emission produced in pulsars could also be interpreted in terms of fast magnetoacoustic wave trains (Karlický 2013).

More advanced models, while still in the plane geometry, accounting for the curvature and longitudinal non-uniformity of the waveguide (or anti-waveguide) showed that the formation of a quasi-periodic fast wave train is a robust feature (Pascoe et al. 2013, 2014) that is well-consistent with observations (Nisticò et al. 2014). Initial perturbations of both sausage and kink symmetries were found to result in quasi-periodic wave trains with the periods prescribed by the fast magnetoacoustic transverse transit time in the vicinity of the initial perturbation. Recent analytical modeling of the evolution of broadband fast waves in a cylindrical waveguide with a step-function transverse profile, which represent, e.g., coronal loops or prominence fibrils, demonstrated the formation of wave trains, too (Oliver et al. 2014, 2015).

The aim of this paper is to study the formation of fast wave trains in a cylindrical waveguide with a smooth transverse profile, investigating the effect of the cylindrical geometry and the waveguide steepness on the wavelet spectral signatures of the wave trains. Our paper is structured as follows: Section 2 describes the numerical setup, and Section 3 presents the simulation results and their discussion. Finally, Section 4 gives the conclusions.

2. NUMERICAL SETUP AND INITIAL CONDITIONS

The simulations were performed using the numerical code Lare3D (Arber et al. 2001). This code solves resistive MHD equations in the normalized Lagrangian form:

$$\frac{D\rho}{Dt} = -\rho \nabla \cdot \boldsymbol{v}, \tag{1}$$

$$\frac{D\boldsymbol{v}}{Dt} = \frac{1}{\rho}(\nabla \times \boldsymbol{B}) \times \boldsymbol{B} - \frac{1}{\rho}\nabla P, \tag{2}$$

$$\frac{D\boldsymbol{B}}{Dt} = (\boldsymbol{B} \cdot \nabla)\boldsymbol{v} - \boldsymbol{B}(\nabla \cdot \boldsymbol{v}) - \nabla \times (\eta \nabla \times \boldsymbol{B}), \tag{3}$$

$$\frac{D\epsilon}{Dt} = -\frac{P}{\rho}\nabla \cdot \boldsymbol{v} + \frac{\eta}{\rho}j^2, \tag{4}$$

where ρ, ϵ, P, $\boldsymbol{v}$, $\boldsymbol{B}$, and $\boldsymbol{j}$ are the mass density, specific internal energy, thermal pressure, velocity, magnetic field, and electric current density, respectively; η is the electrical resistivity. Thermodynamical quantities are linked with each other by the state equation $P = \rho\epsilon(\gamma - 1)$, where γ is the ratio of specific heats. As in this study we are not interested in the dissipative processes, we take $\gamma = 5/3$. The physical quantities were normalized with the use of the following constants: lengths are normalized to $L_0 = 1\,\mathrm{Mm}$, magnetic fields to $B_0 = 20\,\mathrm{G}$, and densities to $\rho_{00} = 1.67 \times 10^{-12}\,\mathrm{kg\,cm^{-3}}$. The mass density normalization corresponds to the electron concentration $n_{e0} = 10^9\,\mathrm{cm^{-3}}$. The normalizing speed was calculated as

$v_0 = B_0/\sqrt{\mu_0\rho_{00}} = 1380\,\mathrm{km\,s^{-1}}$, which is the Alfvén speed corresponding to the values B_0 and ρ_{00}.

The simulations were performed in a 160^3-grid box, which corresponded to the physical volume of $4 \times 4 \times 20\,\mathrm{Mm}$. The resolution was uniform along the Cartesian axes, but different in the directions along and across the magnetic field, allowing us to resolve fine scales in the transverse direction.

Boundary conditions were set to be open (BC_OPEN in Lare3D), which is implemented via far-field Riemann characteristics. The Lare3D authors stressed that the artificial reflection is typically a few percent but can be as large as 10% in extreme cases. In any case, this reflection does not influence the results of our simulations, as our full attention is on the development of the pulse that freely propagates along the cylinder, before it reaches the cylinder's end. In the accompanying movie this perturbation propagates to the left. Hence, this pulse does not experience reflection. In order to test the undesirable effect of the wave reflection from the open x- and y-boundaries we carried out test runs in a computational box with double the resolution, $240 \times 240 \times 160$, and also increasing the computational box in the transverse directions, $6 \times 6 \times 20\,\mathrm{Mm}$. The correlation coefficient between the signals corresponding to the developed wave trains amounted to 99.5%, hence justifying the robustness of the results obtained.

The equilibrium plasma configuration was a plasma cylinder directed along the straight magnetic field, along the z-axis. The cylindrical plasma non-uniformity was implemented by the radial profiles of the physical quantities $B_z(r)$, $n_e(r)$, $T(r)$. We considered cases of steep and smooth boundaries of the cylinder. The case with the step-function profiles (setup1) was implemented with the following plasma parameters: $B_z = 19.5\,\mathrm{G}$, $n_e = 3.3 \times 10^9\,\mathrm{cm^{-3}}$, $T = 9 \times 10^5\,\mathrm{K}$ for $r \leqslant R_0$; and $B_z = 20.0\,\mathrm{G}$, $n_e = 6.6 \times 10^8\,\mathrm{cm^{-3}}$, $T = 2 \times 10^5\,\mathrm{K}$ for $r > R_0$, where $R_0 = 1\,\mathrm{Mm}$ is the cylinder radius.

The cases with smooth profiles (referred to as setup2, setup3, setup4, and setup5) were implemented as follows: the temperature T was constant throughout the whole volume, $n_e(r)$ was given by the generalized symmetric Epstein function (Nakariakov & Roberts 1995; Cooper et al. 2003), and $B_z(r)$ was set to equalize the total pressure everywhere in the computational domain,

$$\begin{cases} n_e(r) = n_\infty + \dfrac{(n_0 - n_\infty)}{\cosh^2\left[(r/R_0)^p\right]} \\ B_z(r) = B_\infty\left(1 - \dfrac{16\pi k_B T(n_0 - n_\infty)}{B_\infty^2 \cosh^2\left[(r/R_0)^p\right]}\right)^{1/2}, \end{cases} \tag{5}$$

where $T = 2 \times 10^5\,\mathrm{K}$, $B_\infty = 20\,\mathrm{G}$, $n_\infty = 6.6 \times 10^8\,\mathrm{cm^{-3}}$, $n_0 = 3.3 \times 10^9\,\mathrm{cm^{-3}}$, k_B is the Boltzmann constant, and p is the parameter controlling the boundary steepness. The specific values of the parameter p and other parameters of the equilibria, corresponding to different numerical setups, are shown in Table 1. The radial profiles of the electron density $n_e(r)$ and magnetic field $B_z(r)$ are depicted in Figure 1. We would like to point out that in all the setups the relative variation of the magnetic field is small, and that the plasma β is much less than unity everywhere.

Dynamics of MHD waves is determined by the Alfvén, $v_A(r) = B_z(r)/\sqrt{\mu_0\rho(r)}$, and sound, $C_S(r) = \sqrt{\gamma P(r)/\rho(r)}$, speeds, where the mass density $\rho(r)$ is prescribed by the

Table 1
Equilibrium Conditions

Title	Profile	B_∞/B_0 (G)	n_∞/n_0 ($\times 10^9$ cm^{-3})	T_∞/T_0 ($\times 10^5$ K)	$v_{A\infty}/v_{A0}$ (km s^{-1})	σ_r (Mm)
setup1	step-function, $p = \infty$	20.0/19.5	0.66/3.3	9.0/2.0	1550/680	0.9
setup2	smooth-profile, $p = 12$	20.0/19.9	0.66/3.3	2.0/2.0	1550/690	0.9
setup3	smooth-profile, $p = 4$	20.0/19.9	0.66/3.3	2.0/2.0	1550/690	0.9
setup4	smooth-profile, $p = 1$	20.0/19.9	0.66/3.3	2.0/2.0	1550/690	0.9
setup5	smooth-profile, $p = 4$	20.0/19.9	0.66/3.3	2.0/2.0	1550/690	0.2

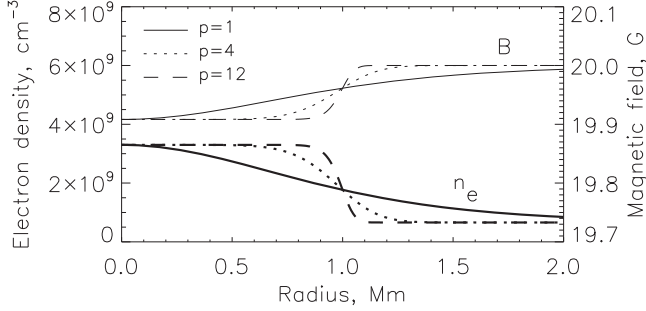**Note.** Parameters of the initial equilibrium in different numerical runs.

Figure 1. Radial profiles of the electron concentration $n_e(r)$ and magnetic field $B_z(r)$ in the simulated plasma cylinder. At the central axis the plasma concentration n_e has a factor of 5 enhancement.

electron concentration $n_e(r)$, and the gas pressure $P(r)$ is determined by the mass density and the temperature using the state equation. In our simulations, the Alfvén speed was $v_{A\infty} = 1550$ km s^{-1} outside the cylinder, and $v_{A0} = 690$ km s^{-1} at the cylinder axis. In *setups2–5* the sound speed was $C_S = 67.6$ km s^{-1} everywhere in the computational domain. In *setup1* the sound speed had the same value at the axis of the cylinder, and was $C_S = 143.4$ km s^{-1} outside the cylinder. We would like to stress that in the low-β plasma that is typical for coronal active regions, the specific value of the sound speed does not affect the parameters of fast magnetoacoustic waves, as their dynamics is controlled by the Alfvén speed.

In all initial setups the fast magnetoacoustic speed determined as $\sqrt{v_A^2(r) + C_S^2(r)}$ had a minimum at the axis of the cylinder. Thus, the plasma cylinder was a refractive waveguide for fast magnetoacoustic waves.

The initial perturbation was set up as a perturbation of the transverse velocity of sausage symmetry,

$$v_r = Ar \exp\left(-\frac{r^2}{2\sigma_r^2}\right)\exp\left(-\frac{(z-z_0)^2}{2\sigma_z^2}\right), \quad (6)$$

where $\sigma_r = 0.9$ Mm for *setup 1*, *setup2*, *setup3*, and *setup4*, and $\sigma_r = 0.2$ Mm for *setup5* (c.f. with the unperturbed radius of the cylinder, $R_0 = 1$ Mm), and $\sigma_z = 0.2$ Mm and $A = 0.1v_0$ for all the setups. The latter condition ensures that nonlinear effects are negligible. The pulse is axisymmetric and hence generates sausage mode perturbations. We placed the pulse near one of the boundaries in the z-direction in order to give more space for the wave train to evolve when it propagates toward the opposite end of the cylinder.

3. RESULTS AND DISCUSSION

Figure 2 shows the shows evolution of a compressive pulse in the plasma cylinder. The initial perturbation develops in a compressive wave that initially propagates radially and obliquely to the axis of the cylinder (see the top central panel), gets partially reflected on gradients of the equilibrium physical parameters, and returns back to the axis of the cylinder (see the top right panel). Then the perturbation overshoots the axis, gets reflected from the opposite boundary, and this scenario repeats again and again (see the bottom panels). Thus, the fast magnetoacoustic perturbation is guided along the axis of the field-aligned plasma cylinder. This phenomenon has been well-known in the solar literature since the pioneering works of Zajtsev & Stepanov (1975) and Edwin & Roberts (1983). For more details the formation of the wave train can be watched in the accompanying movie. The basic physics of this phenomenon is connected with the geometrical dispersion: waves with different wavelengths propagate at different phase and group speeds. Thus, for the same time after the excitation at the same point in the waveguide, different spectral components of the initial excitation travel different distances, and the perturbation becomes "diffused" along the waveguide. Hence, after some time an initially broadband perturbation develops in a quasi-periodic wave train with frequency and amplitude modulation (see, e.g., Nakariakov et al. 2004).

The geometrical dispersion caused by the presence of a characteristic spatial scale in the system, the diameter of the cylinder, leads to the formation of two quasi-periodic fast wave trains propagating in the opposite directions along the axis of the waveguide. This finding is consistent with the analytical results of Oliver et al. (2014, 2015). In the trains, the characteristic parallel wavelengths are comparable by an order of magnitude to the diameter of the waveguide. In the Cartesian coordinates used in the figure, the transverse plasma flows induced by the perturbations are odd functions with respect to the transverse coordinate with the origin at the cylinder's axis. The same structure of the transverse flows is seen in any plane including the axis of the cylinder. In other words the perturbations are independent of the azimuthal angle in the cylindrical coordinates, with the axis coinciding with the axis of the cylinder. The transverse flows vanish to zero at the axis of the cylinder. Thus the excited perturbations are of sausage symmetry, prescribed by the symmetry of the initial perturbation.

The characteristic time signatures of the developed fast magnetoacoustic wave train formed in the waveguides with different equilibrium profiles *setup1*, *setup4*, and *setup5* are shown in Figure 3. In this study we considered only the "direct" wave trains which propagated along the cylinder before they reached its end and experienced reflection (in
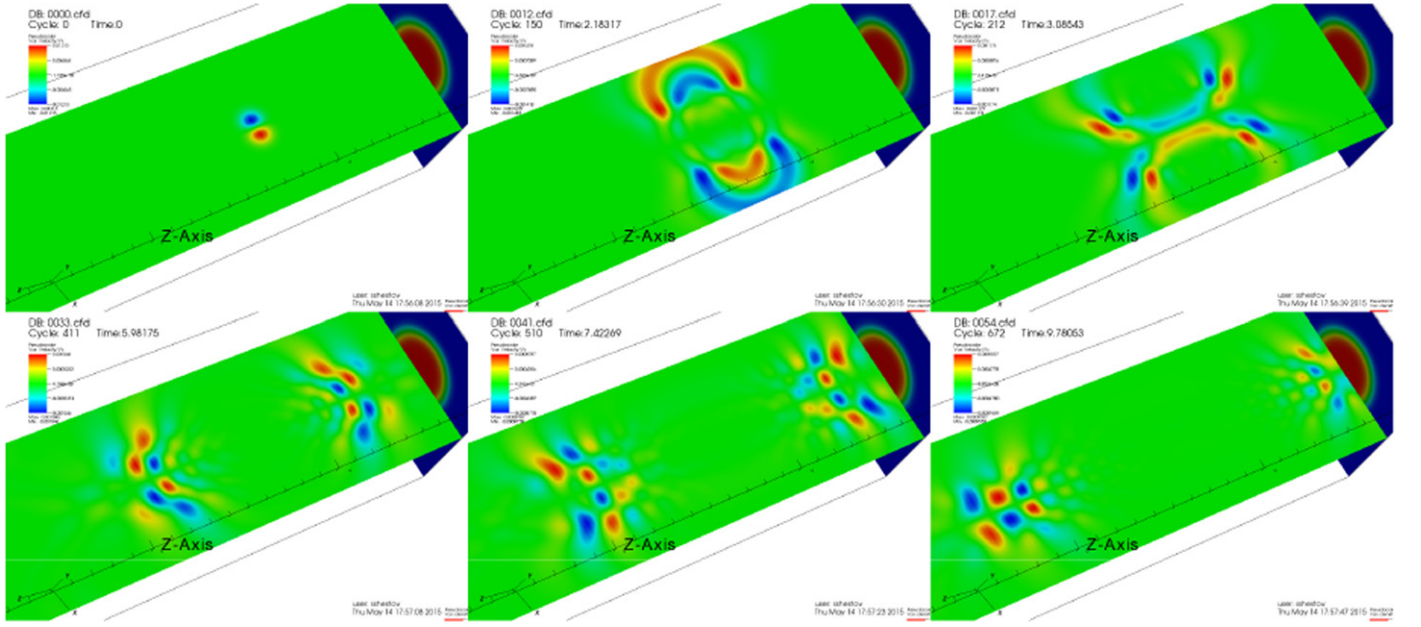
Figure 2. Initial perturbation (upper panels), and the development (lower panels) of fast magnetoacoustic wave trains of sausage symmetry in the magnetic tube, corresponding to *setup5*. The snapshots correspond to the times $t = 0, 2.18, 3.09, 5.98, 7.42, 9.18$ s elapsed after the initial excitation. The horizontal slice, parallel to the cylinder axis along the field, in the *z*-direction, denotes the transverse flow; the perpendicular slice denotes the equilibrium density profile.

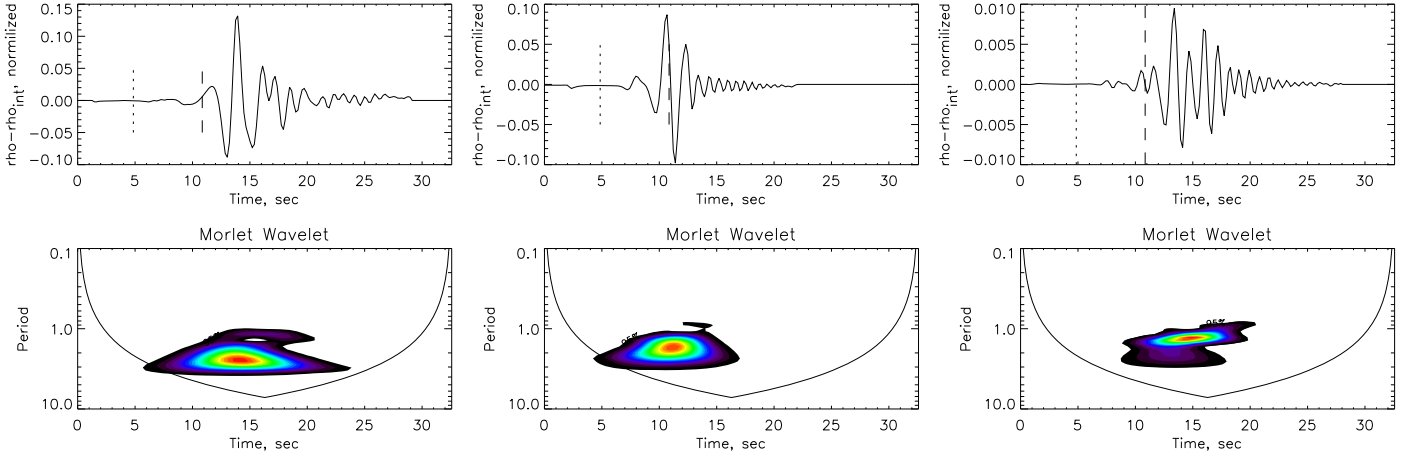(An animation of this figure is available.)

Figure 3. Numerical simulation of an impulsively generated fast magnetoacoustic wave train propagating along a field-aligned plasma cylinder for different numerical setups: left—a sharp (step-function) density profile with $p = \infty$ (*setup1*), middle—smooth density profile with $p = 1$ (*setup4*), and right—smooth density profile with $p = 4$ but with narrower initial perturbation radial size $\sigma_r = 0.2$ (*setup5*). Upper panels: the time evolution of the perturbation of density $\rho(t) - \rho_0$ at the observational point situated at the magnetic tube axis at $h = 7.5$ Mm from the location of the initial perturbation. The vertical lines show the pulse arrival time if the density was uniform: the dotted line corresponds to the fast travel time calculated using the external density ρ_∞, and the dashed line was obtained with the use of the internal density ρ_0. Lower panels: Morlet wavelet transform of the density variation signal at the observational point, demonstrating the characteristic "tadpole" wavelet signature.

Figure 2 and the accompanying movie, it is the wave train propagating to the left). The upper panels show the time evolution of the density measured at the axis at the distance $h = 7.5$ Mm from the initial perturbation location (z_0). The lower panels show the Morlet wavelet spectra of the signals. All signals are seen to have similar features typical for guided fast wave trains: frequency and amplitude modulations, characteristic and cutoff periods, the arrival time determined by $v_{A\infty}$ and the "average" speed determined by $\sim v_{A0}$, dependence of their temporal characteristics on the radial profile of the wave-guiding plasma non-uniformity, and the spatial size of the initial perturbation. All the temporal

characteristics of the wave trains formed in *setup2* and *setup3*, with $p = 12$ and $p = 4$, respectively, are similar to those of *setup1* (the step-function profile) and are not shown here.

The fast wave trains are seen to have a characteristic period of 2–3 s, which is in agreement with the estimate provided by Roberts et al. (1984):

$$P_{\text{prop}} \approx \frac{2\pi R_0}{j_0 \, v_{A0}} \sqrt{1 - \frac{\rho_\infty}{\rho_0}} \approx 3.4 \, \text{s}, \qquad (7)$$

where $j_0 \approx 2.40$ is the first zero of the Bessel function $J_0(x)$.

Sausage modes of a low-β plasma cylinder experience a long-wavelength cutoff (Edwin & Roberts 1983). The spectral components with wavelengths longer than the cutoff value (or with periods longer than the cutoff period) are not trapped in the cylinder and leak out (see, e.g., Cally 1986; Nakariakov et al. 2012; Pascoe et al. 2013). Thus, these spectral components are not present in the spectrum of the guided wave trains. In the case of the step-function profile the cutoff period is

$$P_{\text{cutoff}} = \frac{\sqrt{2}\,\pi R_0}{v_{\text{A0}}}\sqrt{1 - \frac{\rho_\infty}{\rho_0}} \approx 5.7\,\text{s}, \qquad (8)$$

(e.g., Edwin & Roberts 1983). According to the wavelet analysis (Figure 3) the observed maximum period is about 3.5 s, which is roughly consistent with the estimate. The small discrepancy between the theoretical estimate and the numerical result can be attributed to the wave train nature of the signal. Indeed, in the signal the longest period seen in the very beginning of the train lasts for about one cycle of the oscillation only, which leads to effective broadening of the spectrum.

Numerical simulations of the discussed phenomenon, performed for a plasma slab (Nakariakov et al. 2004) and a plane current sheet (Jelínek & Karlický 2012) showed that the wavelet spectra of a developed wave train have a characteristic "crazy tadpole" shape: a long, almost monochromatic tail of low amplitude is followed by a broadband and high-amplitude head (as the tadpole goes tail-first, it was referred to as "crazy"). Another characteristic feature of fast wave trains that formed in waveguides is a pronounced period modulation: the instant period decreases in time. According to the reasoning provided by Roberts et al. (1984) this effect is connected with the geometrical dispersion: longer-wavelength (long period) spectral components propagate at a higher speed, about $v_{\text{A}\infty}$, and hence reach the observational point earlier. In contrast, shorter-wavelength (shorter period) components excited simultaneously and at the same initial location propagate at lower speeds that gradually decrease from the value v_{A0} with the decrease in the wavelength (period) and hence reach the observational point later.

Likewise, the wavelet spectra obtained for cylindrical waveguides, shown in Figure 3 demonstrate the period modulation with the decrease in the instant period with time. The modulation is even better seen in the time signals. As for plane waveguides, wavelet spectra of fast wave trains guided by cylinders have tadpole features too. However, the spectral features either have almost-symmetrical head–tail shapes, or shapes with a broadband "head" occurring at the beginning of the tadpole. Indeed, the time signals of the wave trains show that in the considered case the highest amplitude is reached not near the end of the train, as it is in the slab case, but near its beginning. Thus, one can say that in this case the tadpole goes "head-first," so they are not "crazy." The head of the wave train is seen to propagate at the speed about or slower than the Alfvén speed at the axis of the waveguide, in agreement with the prediction made in Roberts et al. (1984). Thus, we obtain that the characteristic wavelet spectral shapes of fast wave trains are different in the cases of slab and cylinder waveguides. In both geometries the instant period decreases with time, while the amplitude modulation of the trains is different in these two cases. It provides us with a potential tool for the observational

discrimination between these two plasma non-uniformities in the frames of MHD seismology.

Fast wave trains formed in plasma cylinders with smooth radial profiles (with $p < \infty$, *setups 2–5*) are seen to have similar characteristic modulations of the instant amplitude and period. It confirms the robustness of this effect, as it is not very sensitive to the specific shape of the radial profile. Unfortunately, in the cylindrical case we are not aware of the existence of an exact analytical solution of the eigenvalue problem for trapped fast magnetoacoustic waves, similar to the solution described in Nakariakov & Roberts (1995) and Cooper et al. (2003) for the symmetric Epstein transverse profile.

Another interesting feature of the modeling is the appearance of "fins" in the tadpole spectral features (see left panel in Figure 3; similar features are also present in *setup2* and *setup3*, not shown here). The fins are associated with the excitation of the higher radial harmonics. Indeed, it is more pronounced in the case of *setup5*, when the initial pulse has a short size in the radial direction in comparison with the cylinder's radius, $\sigma_z = 0.2 \ll R_0 = 1$. Thus, in this case the spatial radial spectrum of the initial perturbation is broader and less close to the fundamental radial harmonic, leading to the effective excitation of the higher radial harmonics (Nakariakov & Roberts 1995; Mészárosová et al. 2014). The appearance of the "fins" can be readily understood from the dispersion plot (see, e.g., Edwin & Roberts 1983): for the same arrival time, and hence the same group speeds, higher radial harmonics have shorter wavelengths (shorter periods) than the fundamental radial harmonics. This feature is robust and is not qualitatively modified in the case of a smooth radial profile.

4. CONCLUSIONS

We summarize our findings as follows:

1. Dispersive evolution of impulsively generated fast magnetoacoustic waves of sausage symmetry, guided by a plasma cylinder representing, e.g., a coronal loop, a filament fibril, a polar plume, etc., leads to the development of quasi-periodic wave trains. The trains are similar to those found in the plane geometry and also analytically. The wave trains have a pronounced period modulation, with the longer instant period seen in the beginning of the wave train. The wave trains also have a pronounced amplitude modulation. The main characteristics of the wave trains that developed conform mainly with the theoretical and numerical predictions. The wavelet spectra of the wave trains have characteristic tadpole features, with the "heads" preceding the "tails." Similar features have been found in the plane case, although the tadpoles typically go "tail-first" there.

2. The mean period of the wave train is about the transverse fast magnetoacoustic transit time across the cylinder.

3. The mean parallel wavelength is about the diameter of the wave-guiding plasma cylinder.

4. Instant periods are longer than the cutoff period.

5. The wave train characteristics depend on the fast magnetoacoustic speed in both the internal and external media, the smoothness of the transverse profile of the equilibrium quantities, and also the spatial size of the initial perturbation.

6. In the case of the initial perturbation localized at the axis of the cylinder, the wave trains contain not only the

fundamental radial harmonics, but also higher radial harmonics that have shorter periods, but arrive at the remote observational point simultaneously with the fundamental radial harmonic.

We conclude that fast magnetoacoustic wave trains observed in the solar corona in the radio, optical, and EUV bands are a good potential tool for the diagnostics of the wave-guiding plasma structures. The main problem in the implementation of this technique is the need for the information about the initial excitation, which possibly could be excluded when observing the wave train at different locations. This problem is under investigation and will be published elsewhere.

REFERENCES

Arber, T. D., Longbottom, A. W., Gerrard, C. L., & Milne, A. M. 2001, JCoPh, 171, 151

Cally, P. S. 1986, SoPh, 103, 277

Cooper, F. C., Nakariakov, V. M., & Williams, D. R. 2003, A&A, 409, 325

De Moortel, I., & Nakariakov, V. M. 2012, RSPTA, 370, 3193

Edwin, P. M., & Roberts, B. 1983, SoPh, 88, 179

Jelínek, P., & Karlický, M. 2012, A&A, 537, A46

Karlický, M. 2013, A&A, 552, A90

Karlický, M., Jelínek, P., & Mészárosová, H. 2011, A&A, 529, A96

Karlický, M., Mészárosová, H., & Jelínek, P. 2013, A&A, 550, A1

Katsiyannis, A. C., Williams, D. R., McAteer, R. T. J., et al. 2003, A&A, 406, 709

Liu, W., & Ofman, L. 2014, SoPh, 289, 3233

Liu, W., Title, A. M., Zhao, J., et al. 2011, ApJL, 736, L13

Mészárosová, H., Dudík, J., Karlický, M., Madsen, F. R. H., & Sawant, H. S. 2013, SoPh, 283, 473

Mészárosová, H., Karlický, M., Jelínek, P., & Rybák, J. 2014, ApJ, 788, 44

Mészárosová, H., Karlický, M., Rybák, J., & Jiřička, K. 2009, ApJL, 697, L108

Murawski, K., & Roberts, B. 1993, SoPh, 144, 101

Murawski, K., & Roberts, B. 1994, SoPh, 151, 305

Nakariakov, V. M., Arber, T. D., Ault, C. E., et al. 2004, MNRAS, 349, 705

Nakariakov, V. M., Hornsey, C., & Melnikov, V. F. 2012, ApJ, 761, 134

Nakariakov, V. M., Pascoe, D. J., & Arber, T. D. 2005, SSRv, 121, 115

Nakariakov, V. M., & Roberts, B. 1995, SoPh, 159, 399

Nisticò, G., Pascoe, D. J., & Nakariakov, V. M. 2014, A&A, 569, A12

Oliver, R., Ruderman, M. S., & Terradas, J. 2014, ApJ, 789, 48

Oliver, R., Ruderman, M. S., & Terradas, J. 2015, ApJ, 806, 56

Pascoe, D. J., Nakariakov, V. M., & Kupriyanova, E. G. 2013, A&A, 560, A97

Pascoe, D. J., Nakariakov, V. M., & Kupriyanova, E. F. 2012, A&A, 568, A20

Roberts, B., Edwin, P. M., & Benz, A. O. 1983, Natur, 305, 688

Roberts, B., Edwin, P. M., & Benz, A. O. 1984, ApJ, 279, 857

Van Doorsselaere, T., Brady, C. S., Verwichte, E., & Nakariakov, V. M. 2008, A&A, 491, L9

Williams, D. R., Mathioudakis, M., Gallagher, P. T., et al. 2002, MNRAS, 336, 747

Yuan, D., Shen, Y., Liu, Y., et al. 2013, A&A, 554, A144

Zajtsev, V. V., & Stepanov, A. V. 1975, IGAFS, 37, 11